Journal of Materials Chemistry B

PAPER

Cite this: J. Mater. Chem. B, 2019, 7, 4990

In situ formation of metal–organic framework derived CuO polyhedrons on carbon cloth for highly sensitive non-enzymatic glucose sensing†

Siyi Cheng,[abc] Xiang Gao,[ab] Steven DelaCruz,[ab] Chen Chen,[c] Zirong Tang,[c] Tielin Shi,[c] Carlo Carraro[ab] and Roya Maboudian*[ab]

Received 11th June 2019,
Accepted 18th July 2019

DOI: 10.1039/c9tb01166h

rsc.li/materials-b

Metal–organic frameworks (MOFs) are considered promising templates for the fabrication of nanostructured materials with high porosities and high surface areas, which are important parameters for enhanced performance in sensing applications. Here, a facile *in situ* synthetic strategy to construct MOF-derived porous CuO polyhedrons on carbon cloth (CC) is reported. Uniform $Cu(OH)_2$ nanorods are first synthesized on carbon cloth, followed by the conversion of $Cu(OH)_2$ nanorods into porous CuO polyhedrons *via* a copper-based MOF, Cu–BTC, as the intermediate species. When evaluated as a glucose sensing electrode, the as-fabricated CuO polyhedrons/CC composite exhibits a high sensitivity of 13 575 μA mM^{-1} cm^{-2} with a fast response time (t_{90}) of 2.3 s and a low detection limit of 0.46 μM. This work exemplifies the rational fabrication of porous nanostructures on conductive substrates for enhanced performance in glucose detection.

1. Introduction

Developing sensitive and rapid sensors for the quantification of glucose is important in various areas such as clinical diagnostics and the food industry.[1,2] Several approaches, including ones based upon electrochemistry, chemiluminescence, colorimetry, and mass spectrometry, have been explored for the detection of glucose.[3–6] Among these methods, the non-enzymatic electrochemical techniques have attracted much attention due to their robustness, simplicity, and fast response time.[7,8] Over the past decades, transition metals and their composites have been widely used as non-enzymatic glucose sensing materials due to their low cost, enhanced selectivity, and high stability.[9] Particularly, CuO has attracted significant attention for its intrinsic electronic and catalytic properties such as good electrochemical activity and low overpotential for electron transfer reactions.[10,11] It is well known that glucose sensing performance is heavily dependent on the porosity and surface condition of the sensing material.[12] Accordingly, CuO-based nanostructures, including nanowires,[10] nanosheets,[13] nanoparticles,[14] and nanorods,[15] have been constructed to achieve high surface area and well-defined interior voids for improved performance. In comparison, porous 3D nanopolyhedrons are considered to possess superior advantages, including higher specific area, shorter pathways for charge transport, and faster reaction kinetics for glucose oxidation.[16,17]

Metal–organic frameworks, a class of porous hybrid materials comprised of metal ions and organic ligands, have been demonstrated as effective templates for the formation of porous nanostructures.[18–22] In comparisons to other templates, such as polystyrene spheres,[23] bio-templates,[24] and biomass[25] that have been used for the construction of porous structures, MOFs provide unique features including excellent porosity, ordered structures, and controllable morphologies.[26] Recently, various MOF-derived nanostructures, including Ni/NiO porous polyhedrons,[27] Ni_2P/graphene composites,[28] and hexagonal Co_3O_4/graphene,[29] have been reported for glucose sensing. Despite the progress achieved to date, most of the reported MOF-derived porous materials for glucose sensors are limited to powder forms, which necessitate the use of conductive adhesives for immobilization onto the surfaces of conventional electrodes such as glassy carbon or carbon paste electrodes.[30,31] However, such adhesives reduce the active surface area because of the aggregation of the material, which is inevitable in traditional sensor fabrication.[32,33] As such, it would be of great interest to develop *in situ* methods that directly construct MOF-derived nanostructures on conductive substrates, in order to obtain higher surface area and more accessible active sites by avoiding the addition of pore-blocking reagents.

[a] Berkeley Sensor & Actuator Center, University of California, Berkeley, California 94720, USA. E-mail: maboudia@berkeley.edu
[b] Department of Chemical and Biomolecular Engineering, University of California, Berkeley, California 94720, USA
[c] State Key Laboratory of Digital Manufacturing Equipment and Technology, Huazhong University of Science and Technology, Wuhan 430074, China

† Electronic supplementary information (ESI) available. See DOI: 10.1039/c9tb01166h

Here, we report the fabrication of porous CuO polyhedrons on carbon cloth by utilizing Cu MOF as an intermediary. This strategy includes the construction of $Cu(OH)_2$ nanorods on carbon cloth, partial transformation to Cu–BTC *via* the reaction of Cu^{2+} ion and H_3BTC ligand, and calcination to obtain the final CuO structure. This unique fabrication process leads to several advantages. First, three-dimensional flexible carbon cloth is used as a substrate instead of traditional two-dimensional substrates (such as glassy carbon and carbon paste electrodes), offering additional surface area for material growth as well as excellent mechanical strength, high electrical conductivity, and good corrosion resistance. Second, the CuO nanostructures maintain the high-porosity and ordered structure of the MOF precursor, facilitating the penetration of glucose and transportation of ions/electrons. Third, the CuO polyhedrons grown *in situ* on the conductive carbon cloth can be directly used as the electrode without any conductive adhesives. The CuO polyhedrons/CC electrode exhibits excellent glucose sensing performance with high sensitivity, fast response time, low detection limit, and good selectivity.

2. Experimental section

2.1. Fabrication of MOF-derived CuO polyhedrons on carbon cloth

Synthesis of $Cu(OH)_2$ nanorods on carbon cloth: all chemicals were analytical grade and were used without further purification. Carbon cloth, purchased from Cetech Co. Ltd, was cleaned in acetone, ethanol and deionized (DI) water for 10 min each, respectively. After drying in air, carbon cloth was placed into a magnetron sputtering system (TPR-450). A Cu layer was sputtered on both sides of the carbon cloth at a power of 100 W for 30 min. Subsequently, the as-obtained sample was cut into 10 mm × 10 mm pieces and anodized in 3 M NaOH solution at a current density of 10 mA cm^{-2} to form $Cu(OH)_2$ nanorods on carbon cloth.

Synthesis of Cu–BTC/$Cu(OH)_2$ composites on carbon cloth: 0.21 g benzene-1,3,5-tricarboxylic acid (H_3BTC) was dissolved in a solution of 9.4 mL ethanol and 3.6 mL DI water and ultrasonicated for 10 min to form a clear solution.[34] The $Cu(OH)_2$/CC sample was immersed into the above solution at room temperature. After 8 min, the Cu–BTC/$Cu(OH)_2$ on CC product was taken out from the solution and washed with DI water and ethanol and then dried in air.

Synthesis of CuO polyhedrons on carbon cloth: the as-grown Cu–BTC/$Cu(OH)_2$ on CC was placed in a furnace and heated to 350 °C with a ramping rate of 2 °C min^{-1} for 2 h to obtain CuO polyhedrons on carbon cloth.

2.2. Materials characterization

The structures of the as-synthesized samples were characterized by X-ray diffraction (XRD, Bruker AXS D8 Discover with GADDS) using a Co K_α radiation source and by transmission electron microscopy (TEM, JEOL 2010 microscope) under an 80 kV accelerating voltage. The chemical compositions of the samples were analysed using X-ray photoelectron spectroscopy (XPS, Omicron Dar400 system) with an achromatic Al K_α X-ray source. The morphologies and microstructures of the samples were probed by field-emission scanning electronic microscopy (SEM, Zeiss Ultra 60).

2.3. Electrochemical measurements

All electrochemical experiments were performed at room temperature with a CHI 600D electrochemical station. The measurements were performed in 0.1 M NaOH using a conventional three-electrode configuration: carbon cloth samples as the working electrode, Ag/AgCl as the reference electrode, and Pt wire as the counter electrode. For amperometric tests, the solution was stirred to facilitate mixing.

3. Results and discussion

The fabrication process of the Cu–BTC derived CuO polyhedrons on carbon cloth is illustrated in Fig. 1. First, the Cu layer sputtered on carbon cloth was anodized into $Cu(OH)_2$ nanowires in NaOH solution with a galvanostatic method. Then, through a facile reaction of $Cu(OH)_2$ nanorods and benzene-1,3,5-tricarboxylic acid (H_3BTC) ligand, Cu–BTC polyhedral structures were formed *in situ*. Lastly, the $Cu(OH)_2$/Cu–BTC composites were converted to CuO polyhedrons *via* a thermal annealing process in air. The resulting CuO polyhedrons/CC was directly used as the electrode for glucose sensing. Fig. S1 (ESI†) exhibits the color change resulting from the transformation process from Cu to CuO polyhedrons on carbon cloth.

Fig. 2 shows representative XRD spectra obtained on Cu–BTC/$Cu(OH)_2$ composites and CuO polyhedrons on carbon cloth, respectively. The broad diffraction peaks at 25.6° are attributed to the graphitized carbon phase originating from the carbon cloth. The peak located at 43.2° is assigned to (111) plane of cubic Cu (JCPDS 04-0836). As shown in Fig. 2b, except for the peaks arising from the carbon cloth and Cu layer, all the diffraction peaks can be assigned to $Cu(OH)_2$ (JCPDS 13-420) and Cu–BTC[35] (Fig. 2a),

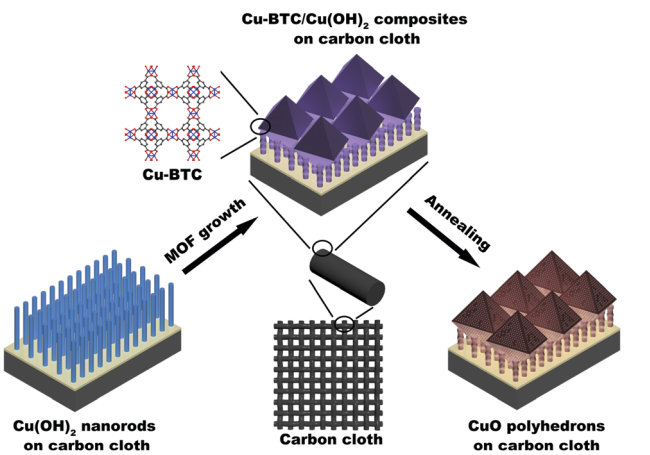

Fig. 1 Schematic of the fabrication process for the Cu–BTC derived CuO polyhedrons on carbon cloth.

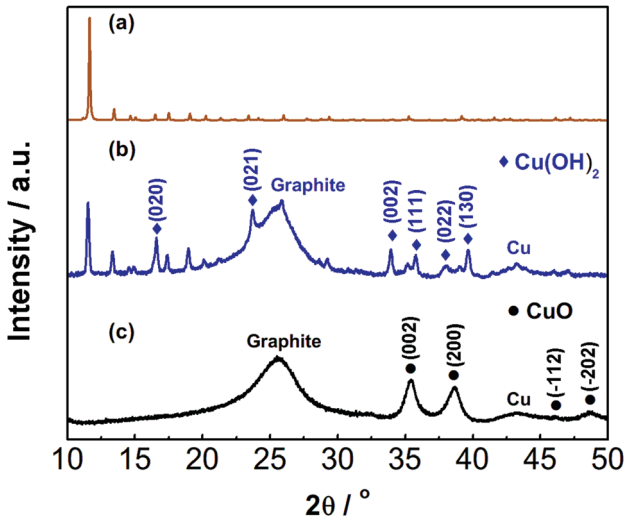

Fig. 2 XRD patterns of (a) simulated Cu–BTC, (b) Cu–BTC/$Cu(OH)_2$ composites, and (c) Cu–BTC derived CuO polyhedrons on carbon cloth.

suggesting the formation of Cu–BTC on $Cu(OH)_2$. After the annealing process, the diffraction peaks (Fig. 2c) at 35.5, 38.7, 46.3, and 48.7° can be indexed to the (002), (200), (−112), and (−202) planes of the monoclinic CuO phase, respectively (JCPDS 5-661). No peaks related to $Cu(OH)_2$ and Cu_2O phases can be found after the annealing process, revealing a complete transformation of Cu–BTC/$Cu(OH)_2$ into CuO.

The near-surface elemental composition and oxidation states of the species on the CuO polyhedrons/CC were measured by XPS. The survey spectrum (Fig. 3a) reveals the co-existence of copper, oxygen and carbon elements on the sample. In the Cu 2p region of the spectrum (Fig. 3b), the two peaks located at the binding energies of 934.1 and 954 eV can be assigned to Cu $2p_{3/2}$ and Cu $2p_{1/2}$, while the shakeup satellite peaks at 942.6 and 962.4 eV can be indexed to Cu^{2+}.[36] As shown in Fig. 3c, the O 1s core-level spectrum is broad, and is fitted to three Gaussian peaks (marked as O1, O2 and O3). The O1 component at the lower energy of 529.9 eV corresponds to O^{2-} binding with Cu. The O2 component at a binding energy of 531.7 eV corresponds to the chemisorbed oxygen on the surface of CuO polyhedrons, and the O3 component at 534.6 eV can be attributed to adsorbed molecular water.[37] The C 1s region of the spectrum (Fig. 3d) can be separated into three components corresponding to carbon atoms in different functional groups: in C–C bonds (285.3 eV) originating from sp^3-hybridized carbon atoms, in C–O bonds (286.4 eV), and the carbonyl and carboxylate C in O–C═O bonds (289.0 eV).[38,39] The XPS results thus confirm the formation of CuO on the carbon substrate, which is in agreement with the XRD result.

The morphologies of the samples at various stages of synthesis were examined by SEM. As shown in Fig. 4a and b, after the anodic oxidation of the Cu layer on carbon cloth, $Cu(OH)_2$ nanorods perpendicular to the carbon cloth surface were formed with an average diameter of ~200 nm. The surface of the $Cu(OH)_2$ nanorods provided Cu^{2+} ions for the formation of Cu–BTC, with the assistance of H_3BTC in an ethanol/DI solution. The reaction between Cu species and H_3BTC induced the transformation of $Cu(OH)_2$ into Cu–BTC with uniform polyhedral structures (Fig. 4c and d). After the calcination of Cu–BTC/$Cu(OH)_2$ composites in air, the overall polyhedron-like

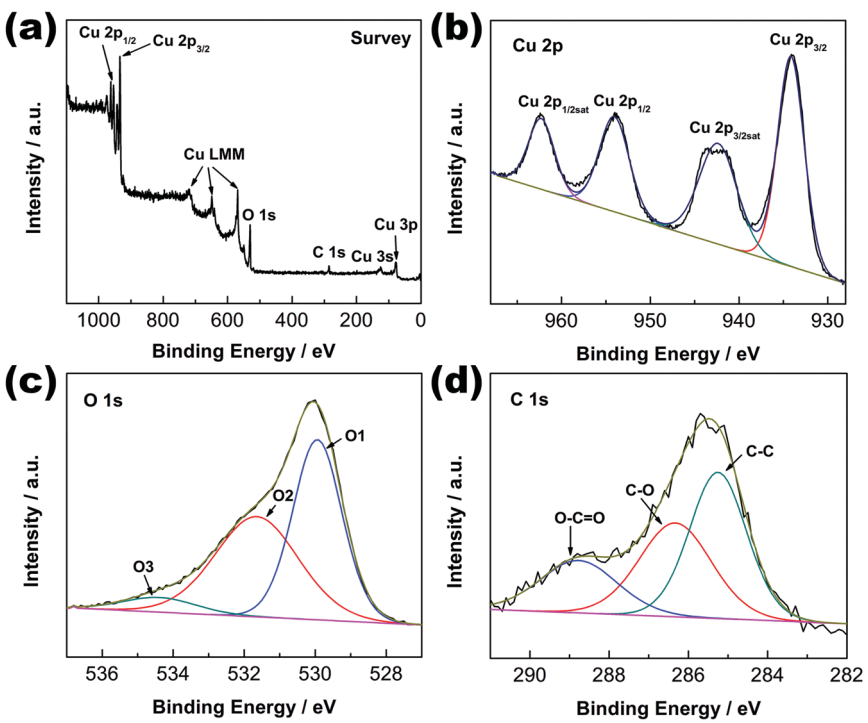

Fig. 3 (a) Survey scan, (b) Cu 2p, (c) O 1s and (d) C 1s regions of the XPS spectrum obtained on the CuO polyhedrons/CC sample.

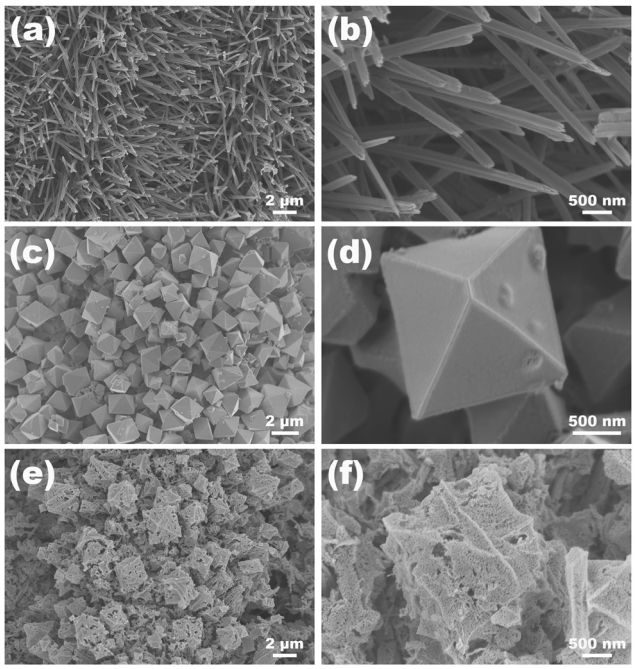

Fig. 4 SEM images at different magnifications obtained on (a and b) $Cu(OH)_2$ nanorods on carbon cloth, (c and d) Cu–BTC/$Cu(OH)_2$ composites on carbon cloth, and (e and f) CuO polyhedrons on carbon cloth.

morphologies were well-preserved (Fig. 4e and f). However, the surface became rougher and an abundance of pores appeared due to the release of the organic ligands during calcination.[40]

The detailed morphologies of the CuO polyhedrons/CC were recorded by TEM. Fig. 5a shows the TEM image of the surface of a CuO polyhedron. The CuO polyhedron is composed of aggregated nanoparticles with a size of ~10 nm, interconnected in a manner that forms a porous structure. The high-resolution TEM (HRTEM) image shown in Fig. 5b displays a crystalline structure. The interplanar distance between adjacent lattice fringes is 0.25 nm, and corresponds well with the (002) lattice plane of CuO, also observed in the XRD spectrum.

To examine the electrochemical performance of the Cu–BTC derived CuO polyhedrons on carbon cloth, non-enzymatic glucose sensing was selected as a model application due to its clinical and industrial significance.[7] Electrochemical tests for different working electrodes were performed using a typical

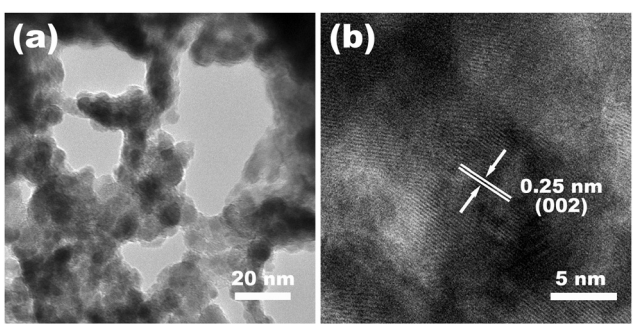

Fig. 5 (a) TEM and (b) HRTEM images of CuO polyhedron/CC.

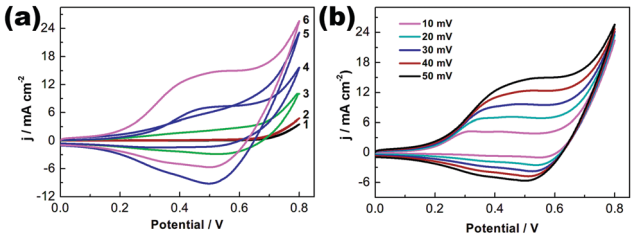

Fig. 6 (a) Cyclic voltammetry curves obtained for bare CC (1, 2), $Cu(OH)_2$ nanorods/CC (3, 4), and CuO polyhedrons/CC (5, 6) in the absence (odd-numbered curves) and presence (even-numbered curves) of 1 mM glucose in 0.1 M NaOH solution at a scan rate of 50 mV s^{-1}. (b) CV responses of CuO polyhedrons/CC electrode in 0.1 M NaOH for different scan rates.

three-electrode configuration in 0.1 M NaOH solution. Fig. 6a displays the cyclic voltammograms (CVs) obtained on bare CC, $Cu(OH)_2$ nanorods/CC, and CuO polyhedrons/CC electrodes in the absence and presence of 1 mM glucose under a scan rate of 50 mV s^{-1}. No obvious peaks can be observed from the bare CC electrode (curve 2) in the presence of glucose (see enlarged CVs in Fig. S2, ESI†), implying negligible contribution from the carbon cloth toward the detection of glucose. The bare CC electrode exhibits a large oxidative tail corresponding to the onset of water splitting observed for potentials above 0.65 V.[41] Broad reduction peaks can be observed for the CuO polyhedrons/CC electrode (curve 5) and $Cu(OH)_2$ nanorods/CC electrode (curve 3) in the absence of glucose. These peaks may correspond to the Cu(III)/Cu(II) redox couple.[42,43] The oxidation peaks related to Cu(II)/Cu(III) are not obvious, which could be due to overshadowing by the oxidation peaks of water-splitting.[41] After the addition of 1 mM glucose, a significant broad peak corresponding to irreversible glucose oxidation can be observed on both electrodes (curves 4 and 6). The broad oxidation peaks from 0.3 to 0.6 V can be attributed to the involvement of Cu(II)/Cu(III) surface species in the oxidation of glucose.[42] It should be noted that the CuO polyhedrons/CC (curve 6) exhibits a higher peak current density than the $Cu(OH)_2$ nanorods/CC (curve 4), indicating an improvement in glucose sensing performance through the transformation from $Cu(OH)_2$ to CuO polyhedrons.

The kinetics of glucose oxidation on the CuO polyhedrons/CC electrode was investigated by the effect of scan rates on the CV response. Fig. 6b exhibits CVs of CuO polyhedrons/CC electrode in 0.1 M NaOH containing 1 mM glucose with scan rates (ν) ranging from 10 to 50 mV s^{-1}. Both anodic (J_{pa}) and cathodic (J_{pc}) peak current densities are found to increase with the scan rate, along with a positive shift of the anodic peaks and a negative shift of the cathodic peaks. The anodic, J_{pa}, and cathodic, J_{pc}, peak current densities show good linearity with the scan rate (Fig. S3, ESI†), and the regression equations can be expressed as J_{pa} (mA cm^{-2}) = 1.56 + 0.26ν (mV s^{-1}) (R^2 = 0.99) and J_{pc} (mA cm^{-2}) = −0.026 − 0.12ν (mV s^{-1}) (R^2 = 0.98), respectively. The linearity implies a surface-controlled electrochemical process on CuO polyhedrons/CC electrode.[44]

To estimate the effective electrochemical surface area (ECSA) during the glucose sensing process, we measured the electrical

double-layer capacitance (EDLC) in 0.1 NaOH solution as the double-layer capacitance (C_{dl}) is proportional to the ECSA.[45] The CV plots were obtained within ±0.05 V of open circuit potential, where the current response should only be due to the charging of the double layer.[46] Fig. S4a and b (ESI†) shows the CV curves of CuO polyhedrons/CC and $Cu(OH)_2$ nanorods/CC electrodes at various scan rates (in 10 to 50 mV s^{-1} range). At each scan rate, the CuO polyhedrons/CC electrode exhibits much higher anodic (j_a) and cathodic (j_c) current densities than the $Cu(OH)_2$ nanorods/CC electrode. As shown in the reported works, the linear slope in such plots is equal to $2C_{dl}$.[47] From $Cu(OH)_2$ nanorods to CuO polyhedrons, the ECSA increased by 5-fold (Fig. S4c, ESI†). This increase might be attributed to the porous structure of Cu–BTC and the pores formed during the calcination process from Cu–BTC to CuO polyhedrons. The porous structure makes the inner area of CuO polyhedrons accessible for glucose sensing.

In order to improve the electrochemical performance of the glucose sensor, the applied potential was optimized using amperometric measurements. Fig. S5a (ESI†) displays the amperometric responses of the CuO polyhedrons/CC electrode upon successive injections of 50 μM glucose into 0.1 M NaOH under different applied potentials from 0.35 V to 0.60 V. The corresponding current density response to glucose injection *versus* applied potential is shown in Fig. S5b (ESI†). The change in current density reaches its highest value at an applied potential of 0.55 V. Thus, the applied potential of 0.55 V is selected as the optimum working potential in subsequent amperometric tests.

Fig. 7a compares the amperometric response of the bare CC, $Cu(OH)_2$ nanorods/CC, and CuO polyhedrons/CC electrodes to successive additions of 50 μM glucose in 0.1 M NaOH at an applied potential of 0.55 V. It is clear that the CuO polyhedrons/CC electrode shows a much higher current density than the $Cu(OH)_2$ nanorods/CC and CC electrodes, which is consistent with the CV results. Fig. 7b shows representative amperometric responses of the CuO polyhedrons/CC electrode to the successive addition of glucose. After glucose was added to the electrolyte, the current response immediately increases and achieves 90% of the steady-state current (t_{90}) within 2.3 s (Fig. S6, ESI†), indicating a fast response to glucose oxidation. The corresponding calibration curve of the CuO polyhedrons/CC electrode is displayed in Fig. 7c. The current density increases linearly with increasing glucose concentration ranging from 0.5 to 800 μM. The sensitivity is 13 575 μA mM^{-1} cm^{-2} with a correlation coefficient of 0.99, and the detection limit is calculated to be 0.46 μM at a signal-to-noise ratio of 3. The CuO polyhedrons/CC electrode exhibits excellent glucose sensing performance, with the highest sensitivity, a lower detection limit and response time, and a comparable linear range, in comparison to the other recently reported CuO based glucose sensors (Table 1). The high sensitivity and fast response time may be attributed to the high conductivity of the carbon cloth, the intimate connection between the active material and the substrate, facilitating electron transfer, and a large contact area offered by Cu–BTC derived CuO polyhedrons for the adsorption of glucose.

Selectivity is another major factor to evaluate the performance of a glucose sensor.[57,58] The selectivity of the CuO polyhedrons/CC electrode was investigated by comparing the amperometric response towards 1 mM glucose, and 0.1 mM interferences including uric acid (UA), ascorbic acid (AA),

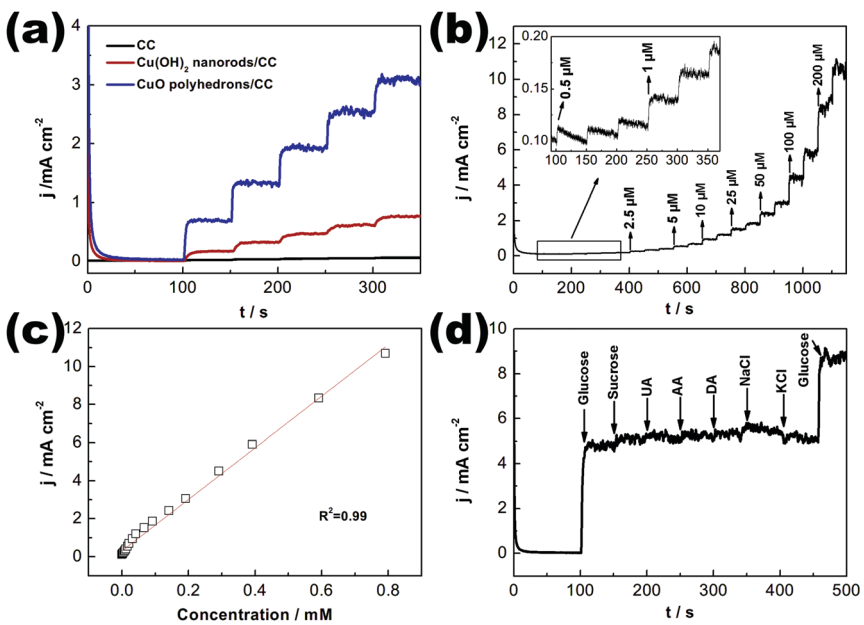

Fig. 7 (a) Amperometric responses of the CC (black), $Cu(OH)_2$ nanorods/CC (red) and CuO polyhedrons/CC (blue) electrodes under successive additions of 50 μM glucose at an applied potential of 0.55 V. (b) Amperometric response of the CuO polyhedrons/CC electrode upon successive additions of glucose with select concentrations marked. Inset: The enlarged view at low concentrations. (c) Calibration curve for glucose of the CuO polyhedrons/CC electrode. (d) Amperometric responses of the CuO polyhedrons/CC electrode to successive additions of glucose and interference species.

Table 1 Comparison of the performance metrics of the CuO polyhedrons/CC electrode with those of earlier reported non-enzymatic glucose sensing electrodes

Electrode material	Sensitivity (μA mM^{-1} cm^{-2})	LOD (μM)	Response time (s)	Linear range (μM)	Ref.
CuO/MWCNTs/GCE	1211	4	3	4–14 500	48
Pt–CuO/GCE	3812	7.5	—	0–600	49
CuO nanoflower/CFF	6476	0.27	1.3	0–960	50
CuO nanosheet/Cu foil	4201	0.5	0.7	0–4000	13
Petal-like CuO/GCE	2634	0.26	1–2	0.5–2670	51
CuO/r-GO/GCE	52.1	0.1	4	0.5–3750	52
Flower-like CuO/SPCE	1460	2.5	—	40–2000	11
CuO nanosheets/CC	4902	1	<3	Up to 1000	53
CuO nanorod/GCE	1523.5	1	<5	Up to 1250	54
CuO nanodisks/SPCE	627.3	0.2	—	2–2500	55
CuO–Au/FTO	2009	0.17	1.6	5–1325	56
CuO polyhedrons/CC	13 575	0.46	2.3	0.5–800	This work

dopamine (DA), sucrose, NaCl and KCl.[59] As depicted in Fig. 7d, 1 mM glucose produces a large response, while 0.1 mM sucrose, UA, AA, DA, NaCl, and KCl yield negligible responses, implying the remarkable selectivity of the CuO polyhedrons/CC electrode as a non-enzymatic glucose sensor. The stability of the CuO polyhedrons/CC electrode was evaluated by measuring the amperometric current response of CuO polyhedrons/CC electrode with the addition of 0.1 mM glucose during a period of 20 days at a time interval of 2 days, as shown in Fig. S7 (ESI†). After 20 days of storage in air, the CuO polyhedrons/CC electrode maintained approximately 99.1% of its original current response, implying a good stability of the CuO polyhedrons. To evaluate the reproducibility of the CuO polyhedrons/CC electrode, we measured the amperometric current response of five CuO polyhedrons/CC electrodes prepared in same condition to the addition of 0.1 mM glucose. The relative standard deviation (RSD) of the current densities is 2.2%, indicating excellent reproducibility.

4. Conclusions

In conclusion, porous CuO polyhedrons were successfully prepared on carbon cloth through an *in situ* conversion strategy in which $Cu(OH)_2$ nanorods were first transformed to Cu–BTC/$Cu(OH)_2$ composites and then oxidized in subsequent calcination process. The CuO polyhedrons/CC was directly used as glucose sensing electrode and showed excellent electrochemical performance with a high sensitivity of 13 575 μA mM^{-1} cm^{-2}, a fast response time (t_{90} = 2.3 s), and a low detection limit of 0.46 μM. This work opens new opportunities for the rational design of porous nanostructures in high-performance electronic devices.

Conflicts of interest

There are no conflicts to declare.

Acknowledgements

The authors thank Jinhu Fan for help with the magnetron sputtering, and Sally Turner for help with the TEM measurements. The support of the industrial members of the Berkeley Sensor & Actuator and National Science Foundation (grant # 1903188) is gratefully acknowledged. Work at the Molecular Foundry was supported by the Office of Science, Office of Basic Energy Sciences, of the U.S. Department of Energy under Contract No. DE-AC02-05CH11231. S. C. acknowledge additional support through the China Scholarship Council. C. C., Z. T. and T.S. acknowledge the National Basic Research Program of China with Project No. 2015CB057205, the Program for Changjiang Scholars and Innovative Research Team in University (Grant No. IRT13017), and the National Science Foundation of China (No. 51775218).

References

1 A. P. Turner, *Chem. Soc. Rev.*, 2013, **42**, 3184–3196.
2 L.-M. Lu, H.-B. Li, F. Qu, X.-B. Zhang, G.-L. Shen and R.-Q. Yu, *Biosens. Bioelectron.*, 2011, **26**, 3500–3504.
3 H. Li, C. Liu, D. Wang and C. Zhang, *Biosens. Bioelectron.*, 2017, **91**, 268–275.
4 M.-Y. Jia, Q.-S. Wu, H. Li, Y. Zhang, Y.-F. Guan and L. Feng, *Biosens. Bioelectron.*, 2015, **74**, 1029–1037.
5 C.-W. Tsao and Z.-J. Yang, *ACS Appl. Mater. Interfaces*, 2015, **7**, 22630–22637.
6 M. Rahman, A. Ahammad, J.-H. Jin, S. J. Ahn and J.-J. Lee, *Sensors*, 2010, **10**, 4855–4886.
7 G. Wang, X. He, L. Wang, A. Gu, Y. Huang, B. Fang, B. Geng and X. Zhang, *Microchim. Acta*, 2013, **180**, 161–186.
8 D.-W. Hwang, S. Lee, M. Seo and T. D. Chung, *Anal. Chim. Acta*, 2018, **1033**, 1–34.
9 X. Niu, X. Li, J. Pan, Y. He, F. Qiu and Y. Yan, *RSC Adv.*, 2016, **6**, 84893–84905.
10 Z. Li, Y. Chen, Y. Xin and Z. Zhang, *Sci. Rep.*, 2015, **5**, 16115.
11 S. G. Leonardi, S. Marini, C. Espro, A. Bonavita, S. Galvagno and G. Neri, *Microchim. Acta*, 2017, **184**, 2375–2385.
12 Q. Guo, L. Liu, M. Zhang, H. Hou, Y. Song, H. Wang, B. Zhong and L. Wang, *Biosens. Bioelectron.*, 2017, **92**, 654–660.
13 R.-m. Yuan, H.-j. Li, X.-m. Yin, J.-h. Lu and L.-l. Zhang, *Talanta*, 2017, **174**, 514–520.
14 Y. Tian, Y. Liu, W.-P. Wang, X. Zhang and W. Peng, *Electrochim. Acta*, 2015, **156**, 244–251.

15 X. Gou, S. Sun, Q. Yang, P. Li, S. Liang, X. Zhang and Z. Yang, *New J. Chem.*, 2018, **42**, 6364–6369.
16 X. Lai, J. E. Halpert and D. Wang, *Energy Environ. Sci.*, 2012, **5**, 5604–5618.
17 W. Huang, Y. Cao, Y. Chen, J. Peng, X. Lai and J. Tu, *Appl. Surf. Sci.*, 2017, **396**, 804–811.
18 B. Liu, H. Shioyama, T. Akita and Q. Xu, *J. Am. Chem. Soc.*, 2008, **130**, 5390–5391.
19 L. Zhang, H. B. Wu, S. Madhavi, H. H. Hng and X. W. Lou, *J. Am. Chem. Soc.*, 2012, **134**, 17388–17391.
20 F. Zou, X. Hu, Z. Li, L. Qie, C. Hu, R. Zeng, Y. Jiang and Y. Huang, *Adv. Mater.*, 2014, **26**, 6622–6628.
21 W. Li, S. Lv, Y. Wang, L. Zhang and X. Cui, *Sens. Actuators, B*, 2019, **281**, 652–658.
22 V. Archana, Y. Xia, R. Fang and G. G. Kumar, *ACS Sustainable Chem. Eng.*, 2019, **7**, 6707–6719.
23 Y. Lian, J. Zhang, X. Ma, P. Yang and M. An, *Ceram. Int.*, 2018, **44**, 2599–2602.
24 J. Ma, H. Fan, H. Tian, X. Ren, C. Wang, S. Gao and W. Wang, *Sens. Actuators, B*, 2018, **262**, 17–25.
25 F. Quan, J. Zhang, D. Li, Y. Zhu, Y. Wang, Y. Bu, Y. Qin, Y. Xia, S. Komarneni and D. Yang, *ACS Sustainable Chem. Eng.*, 2018, **6**, 14911–14918.
26 E. Zhang, Y. Xie, S. Ci, J. Jia and Z. Wen, *Biosens. Bioelectron.*, 2016, **81**, 46–53.
27 H. Yin, J. Zhu, J. Chen, J. Gong and Q. Nie, *Mater. Lett.*, 2018, **221**, 267–270.
28 Y. Zhang, J. Xu, J. Xia, F. Zhang and Z. Wang, *ACS Appl. Mater. Interfaces*, 2018, **10**, 39151–39160.
29 A. E. Vilian, B. Dinesh, M. Rethinasabapathy, S.-K. Hwang, C.-S. Jin, Y. S. Huh and Y.-K. Han, *J. Mater. Chem. A*, 2018, **6**, 14367–14379.
30 B. Haghighi, B. Karimi, M. Tavahodi and H. Behzadneia, *Mater. Sci. Eng., C*, 2015, **52**, 219–224.
31 Z. Amani-Beni and A. Nezamzadeh-Ejhieh, *J. Colloid Interface Sci.*, 2017, **504**, 186–196.
32 L. Zhang, C. Yang, G. Zhao, J. Mu and Y. Wang, *Sens. Actuators, B*, 2015, **210**, 190–196.
33 L. Zhang, Y. Ding, R. Li, C. Ye, G. Zhao and Y. Wang, *J. Mater. Chem. B*, 2017, **5**, 5549–5555.
34 G. Majano and J. Pérez-Ramírez, *Adv. Mater.*, 2013, **25**, 1052–1057.
35 J. L. Zhuang, D. Ceglarek, S. Pethuraj and A. Terfort, *Adv. Funct. Mater.*, 2011, **21**, 1442–1447.
36 Y. Liu, W. Wang, L. Gu, Y. Wang, Y. Ying, Y. Mao, L. Sun and X. Peng, *ACS Appl. Mater. Interfaces*, 2013, **5**, 9850–9855.
37 B. Zhao, H. Yi, X. Tang, Q. Li, D. Liu and F. Gao, *J. Hazard. Mater.*, 2019, **364**, 700–709.
38 J. A. Kim, D. G. Seong, T. J. Kang and J. R. Youn, *Carbon*, 2006, **44**, 1898–1905.
39 J. Yan, T. Wei, B. Shao, F. Ma, Z. Fan, M. Zhang, C. Zheng, Y. Shang, W. Qian and F. Wei, *Carbon*, 2010, **48**, 1731–1737.
40 D. Ji, H. Zhou, Y. Tong, J. Wang, M. Zhu, T. Chen and A. Yuan, *Chem. Eng. J.*, 2017, **313**, 1623–1632.
41 L.-C. Jiang and W.-D. Zhang, *Biosens. Bioelectron.*, 2010, **25**, 1402–1407.
42 G. Liu, B. Zheng, Y. Jiang, Y. Cai, J. Du, H. Yuan and D. Xiao, *Talanta*, 2012, **101**, 24–31.
43 S. Zhou, X. Feng, H. Shi, J. Chen, F. Zhang and W. Song, *Sens. Actuators, B*, 2013, **177**, 445–452.
44 R. Ahmad, N. Tripathy, M. S. Ahn, K. S. Bhat, T. Mahmoudi, Y. Wang, J. Y. Yoo, D. W. Kwon, H. Y. Yang and Y. B. Hahn, *Sci. Rep.*, 2017, **7**, 5715.
45 A. Sivanantham, P. Ganesan and S. Shanmugam, *Adv. Funct. Mater.*, 2016, **26**, 4661–4672.
46 J. Tian, Q. Liu, N. Cheng, A. M. Asiri and X. Sun, *Angew. Chem., Int. Ed.*, 2014, **53**, 9577–9581.
47 F. Song and X. Hu, *Nat. Commun.*, 2014, **5**, 4477.
48 X.-W. Liu, P. Pan, Z.-M. Zhang, F. Guo, Z.-C. Yang, J. Wei and Z. Wei, *J. Electroanal. Chem.*, 2016, **763**, 37–44.
49 N. Myung, S. Kim, C. Lee, T. Kim and K. Rajeshwar, *J. Electrochem. Soc.*, 2016, **163**, B180–B184.
50 W. Xu, S. Dai, X. Wang, X. He, M. Wang, Y. Xi and C. Hu, *J. Mater. Chem. B*, 2015, **3**, 5777–5785.
51 X. Wang, C.-y. Ge, K. Chen and Y. X. Zhang, *Electrochim. Acta*, 2018, **259**, 225–232.
52 J. Zheng, W. Zhang, Z. Lin, C. Wei, W. Yang, P. Dong, Y. Yan and S. Hu, *J. Mater. Chem. B*, 2016, **4**, 1247–1253.
53 Y. Zhong, T. Shi, Z. Liu, S. Cheng, Y. Huang, X. Tao, G. Liao and Z. Tang, *Sens. Actuators, B*, 2016, **236**, 326–333.
54 K. Kim, S. Kim, H. N. Lee, Y. M. Park, Y.-S. Bae and H.-J. Kim, *Appl. Surf. Sci.*, 2019, **479**, 720–726.
55 M. Jagadeesan, K. Movlaee, T. Krishnakumar, S. Leonardi and G. Neri, *J. Electroanal. Chem.*, 2019, **835**, 161–168.
56 P. Chakraborty, S. Dhar, K. Debnath, T. Majumder and S. P. Mondal, *Sens. Actuators, B*, 2019, **283**, 776–785.
57 N. S. Lopa, M. M. Rahman, F. Ahmed, S. C. Sutradhar, T. Ryu and W. Kim, *J. Electroanal. Chem.*, 2018, **822**, 43–49.
58 M. Baghayeri, A. Amiri and S. Farhadi, *Sens. Actuators, B*, 2016, **225**, 354–362.
59 X. Zhang, S. Sun, J. Lv, L. Tang, C. Kong, X. Song and Z. Yang, *J. Mater. Chem. A*, 2014, **2**, 10073–10080.